IEEE Access
Multidisciplinary | Rapid Review | Open Access Journal

Received October 18, 2019, accepted October 28, 2019, date of publication November 6, 2019, date of current version November 20, 2019.

*Digital Object Identifier 10.1109/ACCESS.2019.2951924*

# Multichannel Residual Conditional GAN-Leveraged Abdominal Pseudo-CT Generation via Dixon MR Images

**KE XU[1,2], JIAWEI CAO[1], KAIJIAN XIA[3,2], HUAN YANG[1], JUNQING ZHU[4], CHUNYING WU[4], YIZHANG JIANG[1,2], AND PENGJIANG QIAN[1,2]**

[1]School of Digital Media, Jiangnan University, Wuxi 214122, China
[2]Jiangsu Key Laboratory of Media Design and Software Technology, Jiangnan University, Wuxi 214122, China
[3]Changshu Hospital Affiliated to Soochow University (Changshu No.1 People's Hospital), Changshu 215500, China
[4]Department of Radiology, Case Western Reserve University, Cleveland, OH 44106, USA

Corresponding author: Pengjiang Qian (qianpjiang@jiangnan.edu.cn)

This work was supported in part by the National Natural Science Foundation of China under Grant 61772241 and Grant 61702225, in part by the 2016 Six Talent Peaks Project of Jiangsu Province under Grant 2016-XYDXXJS-014, in part by the 2018 Six Talent Peaks Project of Jiangsu Province under Grant XYDXX-127, in part by the Science and Technology Demonstration Project of Social Development of Wuxi under Grant WX18IVJN002, in part by the Jiangsu Committee of Health on the Subject under Grant H2018071, and in part by the Open Fund Project of Jiangsu Key Laboratory of Media Design and Software Technology (Jiangnan University) under Grant 19ST0205.

**ABSTRACT** Magnetic resonance (MR) images have distinctive advantages in radiation treatment (RT) planning due to their superior, anatomic and functional information compared with computed tomography (CT). For the RT dose calculation, MR images cannot be directly used because of the lack of electron density information. To address this issue, we propose to generate pseudo-CT (pCT) in terms of multiple matching Dixon MR images to support MR-only RT, particularly in the challenging body section of the abdomen. To this end, we design the dedicated multichannel residual conditional generative adversarial network (MCRCGAN). The significance of our efforts is three-fold: 1) The MCRCGAN organically incorporates multiple theories and techniques, such as multichannel residual network (ResNet) and conditional generative adversarial network (cGAN), which facilitate its more authentic pCT generation than many existing methods. 2) The usage of residual modules effectively deepens the network without performance degradation, and the multichannel ResNet helps to simultaneously capture the substance of images, as extensively as possible, which is implicitly contained in the multiple different MR images of the same subject. 3) Due to the designed dedicated network structure, the MCRCGAN is capable of generating satisfactory pCTs under the condition of limited training data as well as prompt prediction response. Experimental studies on ten patients' paired MR-CT images demonstrate the effectiveness of our proposed MCRCGAN model on both the pCT generation quality and the performance stability.

**INDEX TERMS** Generative adversarial network (GAN), pseudo-CT, abdomen, deep learning.

## I. INTRODUCTION

To facilitate reading and understanding, we first list the meanings of the primary abbreviations used throughout this paper in Table 1.

Compared with computed tomography (CT), magnetic resonance imaging (MRI) has superior soft tissue contrast and is therefore widely used in clinic diagnoses. Due to the lack of electron density information, however, MR images are rarely used in isolation in RT planning. Instead, the combination of CT and MR, i.e., their fusion image, is of great significance in both clinical trials and diagnoses in which, for example, CT shows clear bone, whereas MR exhibits high-contrast soft tissue. For precise RT planning, the soft tissue contrast information of MR can be transferred to a patient's CT by registering these two types of medical images. Nonetheless, such a transfer could produce systematic errors due to the potential imperfections and uncertainties of image registration [1]–[3]. For instance, Nakazawa *et al.* [2] demonstrated that the registration of MR and CT could introduce geometrical uncertainties

The associate editor coordinating the review of this manuscript and approving it for publication was Yongtao Hao.

**TABLE 1. Common notations used throughout this manuscript.**

| Abbreviations | Meanings |
|---|---|
| CT | Computed Tomography |
| MR | Magnetic Resonance |
| pCT | Pseudo-CT |
| PET | Positron Emission Tomography |
| AC | Attenuation Correction |
| CNN | Convolutional Neural Network |
| FCN | Fully Convolutional Network |
| GAN | Generative Adversarial Network |
| cGAN | Conditional GAN |
| ResNet | Residual Network |
| MCRCGAN | Multichannel Residual Conditional GAN |

of 0.5 to 2 mm in the brain. To avoid such uncertainties, recent studies have focused on MR-only radiotherapy treatment [4]–[6]. In this regard, effectively generating pseudo-CT (pCT) from given MR images has received an increased amount of research interest [13]. Simulating CT in terms of given MR images can provide benefits from two aspects. On the one hand, patients only need to take MR scans, which allows them to avoid noticeable ionizing radiation. On the other hand, because the generated pCT has the same spatial coordinates as the original MR, the previously intractable issue of imperfect registration no longer exists. In addition, as we revealed in [3], it is important for the attenuation correction (AC) [3], [7] of positron emission tomography (PET) imaging in a hybrid PET/MR system to synthesize a CT based on obtained MR images. PET AC requires the electron density information that CT well indicates, while the intensity value of one voxel in MR images is just dependent on the hydrogen atom density in water.

The specific methods to generate pCT via given MR can be roughly categorized into two groups: traditional technique-based and deep learning-based methods. Traditional techniques include the atlas-used [8], [9], segmentation-used [13], [40], [41], and machine learning-used [3], [10], [16], [42]. Deep learning methods have indicated promising results on image analysis tasks. Convolutional neural network (CNN) [18], [19], a well-known method qualified for image analysis, is commonly employed in multimodality medical image segmentation due to its remarkable ability to capture the potential, complex relationships between inputs and outputs. For example, Zhang *et al.* [20] used a deep CNN to successfully segment infant brain images. As a variation of CNN, fully convolutional network (FCN) can handle image pixels and thus achieves the level of semantic image segmentation. In this regard, Sun *et al.* [21] used a multiple-kernel FCN to automatically segment the liver tumor; Nie *et al.* [22] and Fu *et al.* [23] proposed 2D/3D FCN models to estimate synthetic CT from MRI, respectively. Generative adversarial network (GAN) [24] is another type of fully convolutional model and has also been successfully utilized in image processing. Isola *et al.* [25] proved that the GAN can produce near-real results, such as generating objects from sketches and predicting colors from grayscale images. Kohl *et al.* [26] used the GAN to detect aggressive prostate cancer. Emamic *et al.* [27] generated synthetic CTs from MRI using the GAN, and Kazemifar *et al.* [28] studied the dosimetric accuracy in brain MRI-only radiotherapy using synthetic CTs generated using GAN.

Although existing MR-based, simulated CT generation methods have proven successful for many body sections, such as the brain and pelvis, they seldom show effectiveness in the abdomen, wherein human breath and organ motion often result in image artifacts that greatly increase the difficulty of image analyses [3], [13].

In response to this challenge, in this paper, we introduce a dedicated deep learning architecture, multichannel residual conditional GAN (MCRCGAN for short), to generate pCT from available multiple-modality MR images for the body section of the abdomen. Our contributions lie in the following three aspects:

(1) The MCRCGAN organically incorporates multiple theories and techniques, e.g., multichannel residual network and conditional GAN. Consequently, the pCTs simulated by the MCRCGAN appear more realistic than those simulated by many existing methods.

(2) Residual modules help suppress the issue of performance degradation while greatly deepening our network structure. Additionally, multichannel ResNet is used to mine the substance of multimodality input images as simultaneously and extensively as possible.

(3) Due to the dedicated network structure, the MCRCGAN is able to output satisfactory pCTs under the condition of limited training data as well as prompt prediction response.

The remainder of this manuscript is organized as follows. Related work, e.g., GAN and ResNet, is reviewed briefly in Section II. The proposed MCRCGAN model is introduced specifically in Section III. Experimental studies are presented in Sections IV and V. Conclusions are given in Section VI.

## II. RELATED WORK

### A. GENERATIVE ADVERSARIAL NETWORK

Goodfellow *et al.* [24] first proposed the typical generative adversarial network (GAN), which, in fact, has become a theoretical formula for training models for image simulation currently. A classic GAN consists of two antagonistic networks: the generative network (G) and the discriminant network (D). G inputs a random noise vector and outputs a simulated image. D inputs the simulated image that is generated by G and determines whether it is the real image or the fake one from G. In recent years, many researchers have paid great

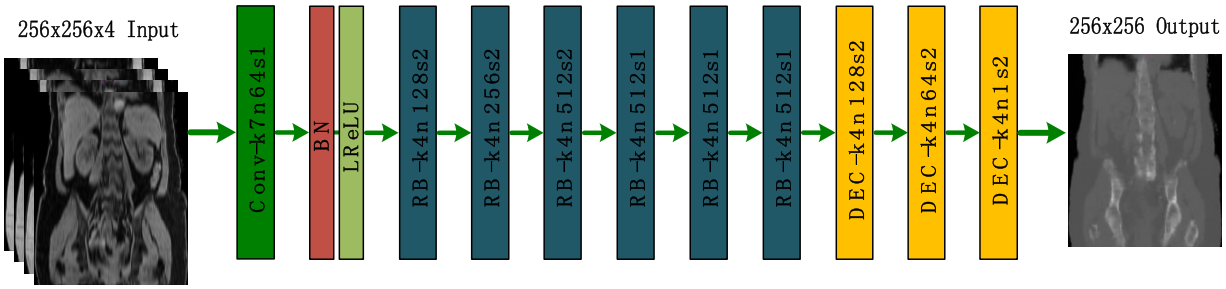


**FIGURE 1.** The architecture of the generator G in the MCRCGAN. The numbers in each rectangle represent the kernel size, number of kernels, and convolution stride, respectively.

attention to GAN, and numerous efforts have been conducted to improve the quality and variability of the generated images from GANs [30], [31].

Conditional GAN [32], [38] (cGAN), employed in this study, is exactly one type of improved GAN. It also contains two opposing networks. The generative network (G) takes the input image $x$ and outputs the generated image $G(x, y)$, in which $y$ could be any conditional information, such as class labels. The discriminant network (D) receives an input image and distinguishes if it is the training image $x$ or the synthesized image $G(x, y)$ generated by the generative network (G). The loss function of cGAN can be represented as

$$L_{cGAN} = E_{x,y\sim Pdata(x,y)}[log(D(x, y))] + E_{x,y\sim Pdata(x,y)}[log(1 - D(G(x, y), y))] \quad (1)$$

where G attempts to minimize the objective function, whereas D attempts to maximize it.

### B. RESIDUAL NETWORK

He *et al.* [29] proposed the residual network (ResNet), and their group won the 2015 ILSVRC competition. Increasing the depth of a neural network usually improves the performance, and conversely, extensive blind deepening is prone to gradient diffusion or gradient explosion. In this context, the ResNet enlists residual blocks and shortcut connections to alleviate the problems of gradient diffusion and gradient explosion while deepening the network architecture.

## III. THE PROPOSED MCRCGAN

To propose an effective deep learning architecture capable of generating satisfactory pseudo-CT from multiple given MR images, we design the dedicated MCRCGAN model that organically incorporates ResNet and multichannel cGAN. The MCRCGAN consists of two parts: the generator (G) and the discriminator (D). G generates the pCT image according to the input multimodality MR images, while D gives the probability that the pCT tends to the real CT. The loss function, used in D to distinguish the generated pseudo-image from the real one and to measure their mismatching degree, is important for the MCRCGAN, as it determines, to a great extent, the efficiency of weight updating during training the network of the MCRCGAN. In view of this, both

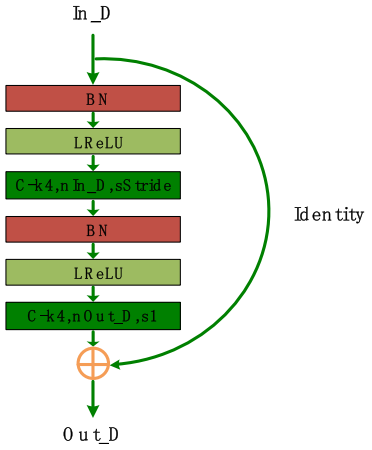


**FIGURE 2.** The structure of the residual block. In_D and Out_D are the dimensions of the input and output data, respectively. The stride is 2 when Out_D is equal to twice In_D or is 1.

the $L_{cGAN}$ loss defined in (1) and the L1 loss indicated in (2) are employed in our study.

$$L_{L_1}(G) = E_{x,y\sim Pdata(x,y)}[||y - G(x, y)||_1] \quad (2)$$

That is, the ultimate loss function used in the MCRCGAN is:

$$L_{MCResCGAN} = L_{cGAN}(G, D) + \lambda L_{L_1}(G) \quad (3)$$

where $\lambda > 0$ is the trade-off factor [25].

Regarding the overall network architecture, the MCRCGAN adopts the multichannel ResNet as the generator, as shown in Fig. 1. Specifically, the generator contains 1 convolution layer (Conv), 6 residual blocks (RB), and 3 deconvolution layers (DEC). Each RB, as further indicated in Fig. 2, is composed of 2 convolution layers (C), each of which follows 1 batch normalization layer (BN) [33] and 1 LeakyReLU nonlinear activation function (LReLU) [34]. Batch normalization is adopted to avoid internal covariate transfer during the training procedure, and LReLU is capable of solving the issues of gradient diffusion and gradient explosion when optimizing the network. For the purpose of obtaining pCT having the same size as the input images, the deconvolution operation is utilized to upsample the intermediate images. The discriminator in the MCRCGAN is generally a regular CNN structure, as detailed in Table 2. It consists of layers

**TABLE 2. Structure of the discriminator D in the MCRCGAN.**

| Layer | Type | Kernel size, number and stride |
|---|---|---|
| 1 | IN-C-LReLU | 4x4, 64, 2 |
| 2 | C-BN-LReLU | 4x4, 128, 2 |
| 3 | C-BN-LReLU | 4x4, 256, 2 |
| 4 | C-BN-LReLU | 4x4, 512, 1 |
| 5 | C-Sigmoid | 4x4, 1, 1 |

**TABLE 3. Patients' MR-CT data for training and testing the MCRCGAN.**

| Repeats | Testing data | | Training data | |
|---|---|---|---|---|
| | Patient | Number of planes | Patients | Number of planes |
| 1 | 1 | 78 | 2-10 | 797 |
| 2 | 2 | 84 | 1, 3-10 | 791 |
| 3 | 3 | 87 | 1-2, 4-10 | 788 |
| 4 | 4 | 92 | 1-3, 5-10 | 783 |
| 5 | 5 | 88 | 1-4, 6-10 | 787 |
| 6 | 6 | 91 | 1-5, 7-10 | 784 |
| 7 | 7 | 91 | 1-6, 8-10 | 784 |
| 8 | 8 | 89 | 1-7, 9-10 | 786 |
| 9 | 9 | 92 | 1-8, 10 | 783 |
| 10 | 10 | 83 | 1-9 | 792 |

of input (IN), convolution (C), batch normalization (BN), LReLU, and sigmoid loss.

## IV. EXPERIMENT

### A. SETUP

Ten sets of MR-CT images were provided by the Department of Radiology, Case Western Reserve University. These images were obtained from 10 volunteers using the modified Dixon (mDixon) MR scan and 120-kV CT scan, respectively. After image reconstruction, we acquired four different types of MR images for each patient: in-phase (IP), opposed-phase (OP), fat, and water. Table 3 lists the training and testing data sets.

Before our experimental studies, each pair of MR-CT images from each patient was subjected to deformable registration [39] to better match their spatial coordinates and to unify their resolutions and fields of view.

To make full use of the training samples, particularly of the available different types of MR images of each patient, the four types of MR images – fat, IP, OP, and water – from 10 patients were simultaneously input into our MCRCGAN model as the multichannel data, as illustrated in Fig. 1. Meanwhile, their corresponding CT image was recruited for the

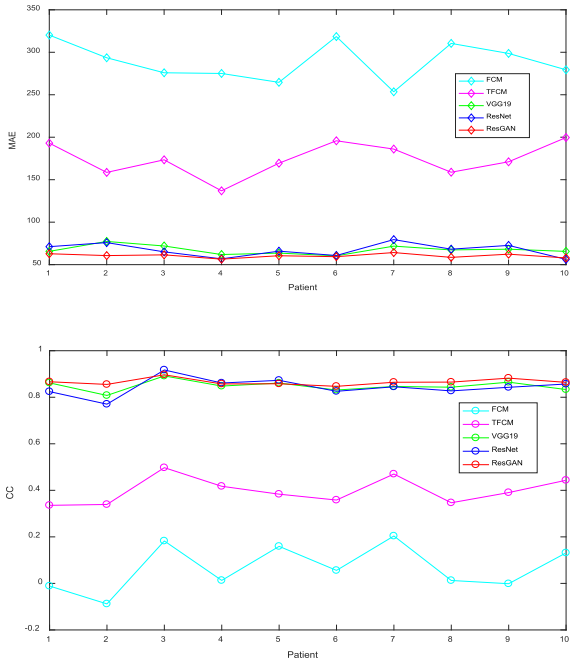


**FIGURE 3. Performance curves of five involved methods in terms of the MAE and CC metrics, respectively.**

discriminator to measure the performance of the generated pseudo-CT via the enlisted loss function (see (3)). For the purpose of further enlarging both the training samples and the data diversity (namely, data augmentation), simple, random image clipping was also used in our experiments. Specifically, every plane of MR images was randomly clipped into many $256 \times 256$ data blocks, and then the input block size became $256 \times 256 \times 4$ after combining the four types of MR.

The leave-one-out strategy was adopted to train and test our network. That is, any nine patients' MR-CT image data were taken as the input to train the network parameters, and the remaining patient's image data were adopted to test the accuracy of our proposed model. For the purpose of performance comparison, in addition to the proposed MCRCGAN, two traditional machine learning methods – FCM [13] and TFCM [35] – and two deep learning methods – VGG19 [36] and ResNet [29] – were employed.

Our experiments were carried out on a workstation with an Intel i7-6850K 3.60 GHz CPU, 128 GB RAM, Nvidia Titan XP GPU, Ubuntu 16.04 (64-bit), and MATLAB 2016b. The MCRCGAN is run in the Google TensorFlow 1.8.0 framework. The number of training epochs was 100, the batch size was 1, and the Adam random gradient descent method [37] was enlisted to minimize the loss function.

### B. VALIDITY METRICS

To measure the accuracy of all involved methods, we need to compare their generated pCTs with the real CTs that were obtained from the abdomens of all patients. To this end, we first spliced all the pCT planes for each patient and then regenerated a 3D volume. The metrics of mean absolute error

**TABLE 4.** Quantitative comparisons of the proposed MCRCGAN and the other competitors.

| Sub | | | 1 | 2 | 3 | 4 | 5 | 6 | 7 | 8 | 9 | 10 |
|---|---|---|---|---|---|---|---|---|---|---|---|---|
| MAE | FCM | Mean | 319.06 | 292.53 | 274.22 | 273.86 | 263.36 | 315.99 | 252.19 | 308.81 | 297.55 | 276.56 |
| | | std | 8.14E-05 | 2.03E-05 | 1.03E-04 | 3.22E-05 | 0 | 1.07E-04 | 1.19E-04 | 4.32E-05 | 3.22E-05 | 7.49E-04 |
| | TFCM | Mean | 189.81 | 155.83 | 170.1 | 133.46 | 165.81 | 192.36 | 182.69 | 155.67 | 167.98 | 195.74 |
| | | std | 1.61E-05 | 1.61E-05 | 1.61E-05 | 1.61E-05 | 1.61E-05 | 1.61E-05 | 0 | 5.69E-05 | 0 | 1.61E-05 |
| | VGG19 | Mean | 65.63 | 77.30 | 71.95 | 61.90 | 63.57 | 60.37 | 71.78 | 67.33 | 68.18 | 65.59 |
| | | std | 0 | 0 | 0 | 0 | 0 | 0 | 0 | 0 | 0 | 0 |
| | ResNet | Mean | 71.14 | 75.93 | 65.03 | 56.82 | 65.84 | 60.76 | 79.46 | 68.19 | 72.63 | 56.19 |
| | | std | 0 | 0 | 0 | 0 | 0 | 0 | 0 | 0 | 0 | 0 |
| | MCRCGAN | Mean | 62.81 | 60.64 | 61.51 | 56.46 | 60.46 | 59.36 | 64.21 | 58.56 | 62.32 | 57.89 |
| | | std | 0 | 0 | 0 | 0 | 0 | 0 | 0 | 0 | 0 | 0 |
| CC | FCM | Mean | -0.01 | -0.09 | 0.18 | 0.01 | 0.16 | 0.06 | 0.21 | 0.01 | -2.69E-04 | 0.13 |
| | | std | 1.59E-07 | 4.95E-08 | 5.54E-07 | 0 | 0 | 1.51E-07 | 6.03E-07 | 7.36E-08 | 3.07E-11 | 5.99E-07 |
| | TFCM | Mean | 0.34 | 0.34 | 0.50 | 0.42 | 0.38 | 0.36 | 0.47 | 0.35 | 0.39 | 0.44 |
| | | std | 3.14E-08 | 3.44E-08 | 6.28E-08 | 6.28E-08 | 0 | 4.44E-08 | 3.97E-08 | 3.14E-08 | 9.93E-08 | 3.44E-08 |
| | VGG19 | Mean | 0.86 | 0.81 | 0.89 | 0.85 | 0.86 | 0.83 | 0.85 | 0.84 | 0.86 | 0.83 |
| | | std | 0 | 0 | 0 | 0 | 0 | 0 | 0 | 0 | 0 | 0 |
| | ResNet | Mean | 0.82 | 0.77 | 0.92 | 0.86 | 0.87 | 0.83 | 0.84 | 0.83 | 0.84 | 0.86 |
| | | std | 0 | 0 | 0 | 0 | 0 | 0 | 0 | 0 | 0 | 0 |
| | MCRCGAN | Mean | 0.87 | 0.86 | 0.90 | 0.86 | 0.86 | 0.85 | 0.86 | 0.87 | 0.88 | 0.86 |
| | | std | 0 | 0 | 0 | 0 | 0 | 0 | 0 | 0 | 0 | 0 |

(MAE, defined in (4)) and Pearson correlation coefficient (CC) were calculated to quantitatively assess the performance of all methods.

$$MAE = \frac{1}{N}\sum_{i=1}^{N} |CT(i) - sCT\ (i)\ | \tag{4}$$

where $N$ is the total voxel number in the CT volume and $CT(i)$ and $sCT(i)$ denote the intensity value of voxel $i$ in the real CT and pCT, respectively. Smaller MAE values indicate better quality of pCT. The value of CC is within $[-1, 1]$, and the closer its absolute value is to 1, the stronger the correlation is.

### C. RESULTS

After separately running FCM, TFCM, VGG19, ResNet, and the MCRCGAN with the experimental data listed in Table 3, the quantitative results obtained are listed in Table 4, measured in terms of the MAE and CC metrics. Based on these results, we illustrate the performance curves for all involved methods in Fig. 3. For the pCTs output by these 5 methods, in view of the limitation of paper length, we only present the outcomes on Patient 4, as shown in Fig. 4. To distinctly demonstrate the advantages of our proposed method, the average percentage improvements of the MCRCGAN against the other methods on all patients are further indicated in Table 5.

**TABLE 5.** The average percentage improvements of the MCRCGAN (%).

| | FCM | TFCM | ResNet | VGG19 |
|---|---|---|---|---|
| MAE | 78.96 | 64.97 | 9.29 | 9.96 |
| CC | 92.45 | 54.05 | 2.47 | 1.94 |

## V. DISCUSSION

As revealed in Table 4, the MCRCGAN achieves considerable performance improvements versus traditional machine learning methods, such as FCM and TFCM. Regarding the deep learning methods, the MCRCGAN surpasses VGG19, particularly in terms of the MAE index. Compared with ResNet, the MCRCGAN also generally exhibits better or comparable performance. In addition, as shown in Fig. 3, the MCRCGAN shows preferable performance stability compared with the other four approaches through the 10 patients' image data.

Fig. 4 shows that both FCM and TFCM, two conventional fuzzy clustering approaches, do not work correctly on bone. In contrast, the produced pCT of the MCRCGAN is distinctly clearer than the others, especially on the bone tissue.

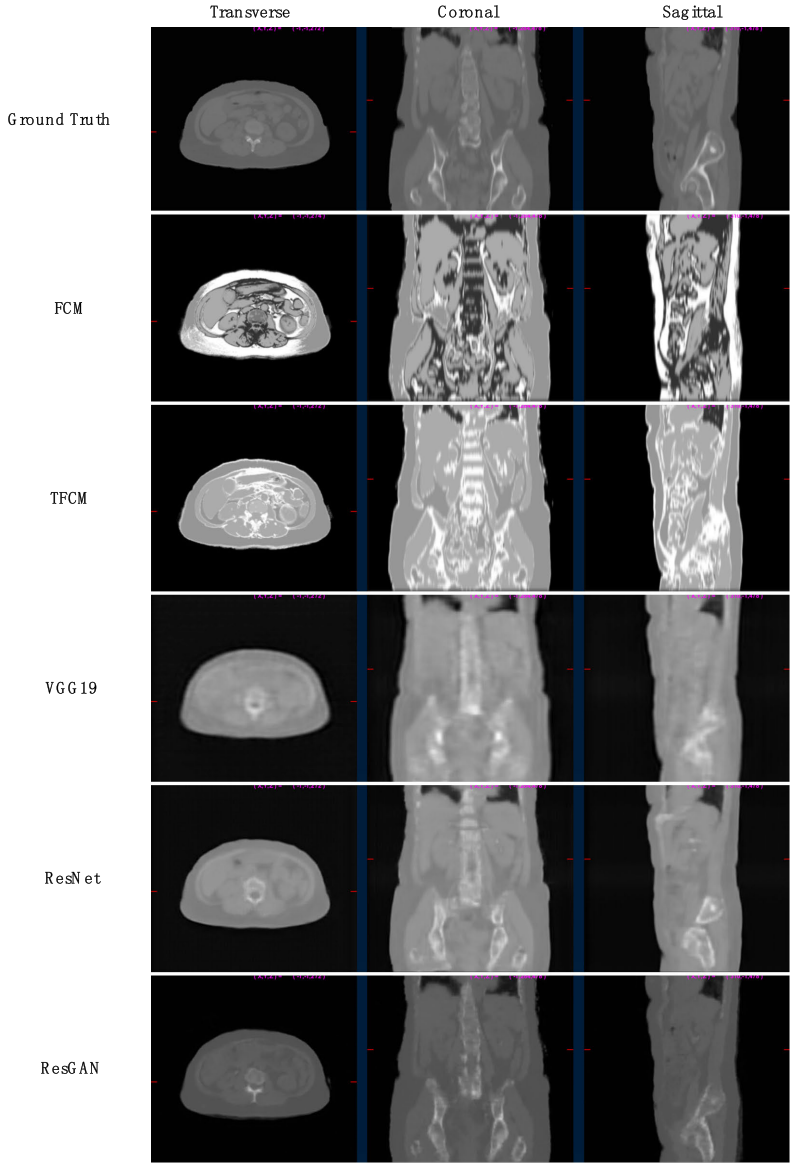


**FIGURE 4.** Abdominal real CT and pCTs generated by five methods on Patient 4.

In contrast to traditional neural networks that usually require large numbers of training samples, our MCRCGAN is capable of producing acceptable pCTs with a limited quantity of training data.

Moreover, one of the advantages of the MCRCGAN is that it can be deployed quickly. Although we currently spend approximately 2 hours to train the network, this process can be accelerated using multiple GPUs. For a new patient, only approximately 3 seconds are needed to obtain the pCT through the well-trained MCRCGAN model, and this benefits clinical applications to a certain extent.

## VI. CONCLUSION

In this paper, we present the deep learning model MCRCGAN based on cGAN and multichannel ResNet to generate abdominal pseudo-CT from multiple given MR images. Experimental studies demonstrate that our proposed method is able to estimate excellent pCT with a limited number of training samples as well as a relatively prompt prediction. The high-quality pCT generation together with low computational costs ensures the practicability of clinical applications of our method, especially for the challenging abdomen.

In the near future, one pathway could be used to further improve the accuracy of the proposed MCRCGAN, that is, to train three different MCRCGAN models from three directions, transverse, coronal, and sagittal, on each patient's MR volumes according to the corresponding image planes. Then, for a new patient, each of the obtained MCRCGAN models would output an intermediate pCT, and the eventual pCT would be regenerated by properly assembling these intermediate pCTs, such as via the weighted average strategy.

## REFERENCES


[1] K. Ulin, M. M. Urie, and J. M. Cherlow, "Results of a multi-institutional benchmark test for cranial CT/MR image registration," *Int. J. Radiat. Oncol. Biol. Phys.*, vol. 77, no. 5, pp. 1584–1589, 2010.

[2] H. Nakazawa, Y. Mori, M. Komori, Y. Shibamoto, T. Tsugawa, T. Kobayashi, and C. Hashizume, "Validation of accuracy in image co-registration with computed tomography and magnetic resonance imaging in Gamma Knife radiosurgery," *J. Radiat. Res.*, vol. 55, no. 5, pp. 924–933, 2014.

[3] P. Qian, Y. Chen, J.-W. Kuo, Y.-D. Zhang, Y. Jiang, K. Zhao, R. A. Helo, H. Friel, A. Baydoun, F. Zhou, J. U. Heo, N. Avril, K. Herrmann, R. Ellis, B. Traughber, R. S. Jones, S. Wang, K.-H. Su, and R. F. Muzic, Jr., "mDixon-based synthetic CT generation for PET attenuation correction on abdomen and pelvis jointly using transfer fuzzy clustering and active learning-based classification," *IEEE Trans. Med. Imag.*, to be published, doi: 10.1109/TMI.2019.2935916.

[4] B. Demol, C. Boydev, J. Korhonen, and N. Reynaert, "Dosimetric characterization of MRI-only treatment planning for brain tumors in atlas-based pseudo-CT images generated from standard T1-weighted MR images," *Med. Phys.*, vol. 43, no. 12, pp. 6557–6568, Dec. 2016.

[5] Y. Yang, M. Cao, T. Kaprealian, K. Sheng, Y. Gao, F. Han, C. Gomez, A. Santhanam, S. Tenn, N. Agazaryan, D. A. Low, and P. Hu, "Accuracy of UTE-MRI-based patient setup for brain cancer radiation therapy," *Med. Phys.*, vol. 43, no. 1, pp. 262–267, 2016.

[6] J. H. Jonsson, M. M. Akhtari, M. G. Karlsson, A. Johansson, T. Asklund, and T. Nyholm, "Accuracy of inverse treatment planning on substitute CT images derived from MR data for brain lesions," *Radiat. Oncol.*, vol. 10, Jan. 2015, Art. no. 13.

[7] M. Hofmann, B. Pichler, B. Schölkopf, and T. Beyer, "Towards quantitative PET/MRI: A review of MR-based attenuation correction techniques," *Eur. J. Nucl. Med. Mol. Imag.*, vol. 36, pp. s93–s104, Mar. 2009.

[8] J. Sjölund, D. Forsberg, M. Andersson, and H. Knutsson, "Generating patient specific pseudo-CT of the head from MR using atlas-based regression," *Phys. Med. Biol.*, vol. 60, no. 2, pp. 825–839, 2015.

[9] J. A. Dowling, J. Lambert, J. Parker, O. Salvado, J. Fripp, A. Capp, C. Wratten, J. W. Denham, and P. B. Greer, "An atlas-based electron density mapping method for magnetic resonance imaging (MRI)-alone treatment planning and adaptive MRI-based prostate radiation therapy," *Int. J. Radiat. Oncol. Biol. Phys.*, vol. 83, no. 1, pp. e5–e11, May 2012.

[10] J. A. Dowling, J. Sun, P. Pichler, D. Rivest-Hénault, S. Ghose, H. Richardson, C. Wratten, J. Martin, J. Arm, L. Best, S. S. Chandra, J. Fripp, F. W. Menk, and P. B. Greer, "Automatic substitute computed tomography generation and contouring for magnetic resonance imaging (MRI)-alone external beam radiation therapy from standard MRI sequences," *Int. J. Radiat. Oncol. Biol. Phys.*, vol. 93, no. 5, pp. 1144–1153, 2015.

[11] C. Catana, A. van der Kouwe, T. Benner, C. J. Michel, M. Hamm, M. Fenchel, B. Fischi, B. Rosen, M. Schmand, and A. G. Sorensen, "Toward implementing an MRI-based PET attenuation-correction method for neurologic studies on the MR-PET brain prototype," *J. Nucl. Med.*, vol. 51, no. 9, pp. 1431–1438, Sep. 2010.

[12] A. Martinez-Möller, M. Souvatzoglou, G. Delso, R. A. Bundschuh, C. Chefd'hotel, S. I. Ziegler, N. Navab, M. Schwaiger, and S. G. Nekolla, "Tissue classification as a potential approach for attenuation correction in whole-body PET/MRI: Evaluation with PET/CT data," *J. Nucl. Med.*, vol. 50, no. 4, pp. 520–526, 2009.

[13] K. H. Su, L. Hu, C. Stehning, M. Helle, P. Qian, C. L. Thompson, G. C. Pereira, D. W. Jordan, K. A. Herrmann, M. Traughber, R. F. Muzic, Jr., and B. J. Traughber, "Generation of brain pseudo-CTs using an undersampled, single-acquisition UTE-mDixon pulse sequence and unsupervised clustering," *Med. Phys.*, vol. 42, no. 8, pp. 4974–4986, Aug. 2015.

[14] V. Keereman, Y. Fierens, T. Broux, Y. De Deene, M. Lonneux, and S. Vandenberghe, "MRI-based attenuation correction for PET/MRI using ultrashort echo time sequences," *J. Nucl. Med.*, vol. 51, no. 5, pp. 812–818, May 2010.

[15] Y. Berker, J. Franke, A. Salomon, M. Palmowski, C. H. Donker, Y. Temur, F. M. Mottaghy, C. Kuhl, D. Izquierdo-Garcia, Z. A. Fayad, F. Kiessling, and V. Schulz, "MRI-based attenuation correction for hybrid PET/MRI systems: A 4-class tissue segmentation technique using a combined ultrashort-echo-time/Dixon MRI sequence," *J. Nucl. Med.*, vol. 53, no. 5, pp. 796–804, May 2012.

[16] T. Huynh, Y. Gao, J. Kang, L. Wang, P. Zhang, and J. Lian, "Estimating CT image from MRI data using structured random forest and auto-context model," *IEEE Trans. Med. Imag.*, vol. 35, no. 1, pp. 174–183, Jan. 2016.

[17] X. Yang, Y. Lei, H.-K. Shu, R. Peter, H. Mao, H. Shim, W. J. Curran, and T. Liu, "Pseudo CT estimation from MRI using patch-based random forest," *Proc. SPIE*, vol. 10133, Feb. 2017, Art. no. 101332Q.

[18] Y. LeCun, Y. Bengio, and G. Hinton, "Deep learning," *Nature*, vol. 521, pp. 436–444, May 2015.

[19] Y. Lecun, L. Bottou, Y. Bengio, and P. Haffner, "Gradient-based learning applied to document recognition," *Proc. IEEE*, vol. 86, no. 11, pp. 2278–2324, Nov. 1998.

[20] W. Zhang, R. Li, H. Deng, L. Wang, W. Lin, S. Ji, and D. Shen, "Deep convolutional neural networks for multi-modality isointense infant brain image segmentation," *NeuroImage*, vol. 108, pp. 214–224, Mar. 2015.

[21] C. Sun, S. Guo, H. Zhang, J. Li, S. Ma, and X. Li, "Liver lesion segmentation in CT images with MK-FCN," in *Proc. IEEE 2nd Adv. Inf. Technol., Electron. Automat. Control Conf. (IAEAC)*, Mar. 2017, pp. 1794–1798.

[22] D. Nie, X. Cao, Y. Gao, L. Wang, and D. Shen, "Estimating CT image from MRI data using 3D fully convolutional networks," in *Deep Learning and Data Labeling for Medical Applications*. Cham, Switzerland: Springer, 2016, pp. 170–178.

[23] J. Fu, Y. Yang, K. Singhrao, D. Ruan, D. A. Low, and J. H. Lewis, "Male pelvic synthetic CT generation from T1-weighted MRI using 2D and 3D convolutional neural networks," *Med. Phys.*, vol. 46, no. 9, pp. 3788–3798, 2019.

[24] I. J. Goodfellow, J. Pouget-Abadie, M. Mirza, B. Xu, D. Warde-Farley, S. Ozair, A. Courville, and Y. Bengio, "Generative adversarial nets," in *27th Int. Conf. Neural Inf. Process. Syst.*, vol. 2, 2014, pp. 2672–2680.

[25] P. Isola, J.-Y. Zhu, T. Zhou, and A. A. Efros, "Image-to-image translation with conditional adversarial networks," in *Proc. IEEE Conf. Comput. Vis. Pattern Recognit.*, Jul. 2017, pp. 5967–5976.

[26] S. Kohl, D. Bonekamp, H.-P. Schlemmer, K. Yaqubi, M. Hohenfellner, B. Hadaschik, J. P. Radtke, and K. Maier-Hein, "Adversarial networks for the detection of aggressive prostate cancer," Feb. 2017, *arXiv:1702.08014*. [Online]. Available: https://arxiv.org/abs/1702.08014

[27] H. Emami, M. Dong, S. P. Nejad-Davarani, and C. K. Glide-Hurst, "Generating synthetic CTs from magnetic resonance images using generative adversarial networks," *Med. Phys.*, vol. 45, no. 8, pp. 3627–3636, 2018.

[28] S. Kazemifar, S. McGuire, R. Timmerman, Z. Wardak, D. Nguyen, Y. Park, S. Jiang, and A. Owrangi, "MRI-only brain radiotherapy: Assessing the dosimetric accuracy of synthetic CT images generated using a deep learning approach," *Radiotherapy Oncol.*, vol. 136, pp. 56–63, Jul. 2019.

[29] K. He, X. Zhang, S. Ren, and J. Sun, "Deep residual learning for image recognition," in *Proc. IEEE Conf. Comput. Vis. Pattern Recognit.*, Jun. 2016, pp. 770–778.

[30] M. Arjovsky, S. Chintala, and L. Bottou, "Wasserstein generative adversarial networks," in *Proc. 34th Int. Conf. Mach. Learn.*, vol. 70, 2017, pp. 214–223.

[31] D. Berthelot, T. Schumm, and L. Metz, "BEGAN: Boundary equilibrium generative adversarial networks," May 2017, *arXiv:1703.10717*. [Online]. Available: https://arxiv.org/abs/1703.10717

[32] M. Mirza and S. Osindero, "Conditional generative adversarial nets," Nov. 2014, *arXiv:1411.1784*. [Online]. Available: https://arxiv.org/abs/1411.1784

[33] S. Ioffe and C. Szegedy, "Batch normalization: Accelerating deep network training by reducing internal covariate shift," in *Proc. 32nd Int. Conf. Mach. Learn.*, vol. 37, Feb. 2015, pp. 448–456.

[34] A. L. Maas, A. Y. Hannun, and A. Y. Ng, "Rectifier nonlinearities improve neural network acoustic models," in *Proc. 30th Int. Conf. Mach. Learn.*, vol. 30, 2013, pp. 1–6.

[35] P. Qian, S. Sun, Y. Jiang, K.-H. Su, T. Ni, S. Wang, and R. F. Muzic, Jr., "Cross-domain, soft-partition clustering with diversity measure and knowledge reference," *Pattern Recognit.*, vol. 50, pp. 155–177, Feb. 2016.

[36] K. Simonyan and A. Zisserman, "Very deep convolutional networks for large-scale image recognition," Sep. 2014, *arXiv:1409.1556*. [Online]. Available: https://arxiv.org/abs/1409.1556

[37] D. P. Kingma and J. Ba, "Adam: A method for stochastic optimization," Dec. 2014, *arXiv:1412.6980*. [Online]. Available: https://arxiv.org/abs/1412.6980

[38] P. Wang and X. Bai, "Thermal infrared pedestrian segmentation based on conditional GAN," *IEEE Trans. Image Process.*, vol. 28, no. 12, pp. 6007–6021, Dec. 2019.

[39] G. Janssens, L. Jacques, J. O. de Xivry, X. Geets, and B. Macq, "Diffeomorphic registration of images with variable contrast enhancement," *Int. J. Biomed. Imag.*, vol. 2011, Dec. 2010, Art. no. 891585.

[40] S. Hsu, Y. Cao, and J. Balter, "MO-G-BRA-02: Investigation of a method for generating synthetic CT models from MRI scans for radiation therapy," *Med. Phys.*, vol. 39, p. 3881, Jun. 2012.

[41] M. Khalifé, B. Fernandez, O. Jaubert, M. Soussan, V. Brulon, I. Buvat, and C. Comtat, "Subject-specific bone attenuation correction for brain PET/MR: Can ZTE-MRI substitute CT scan accurately?" *Phys. Med. Biol.*, vol. 62, no. 19, pp. 7814–7832, 2017.
[42] A. Jog, A. Carass, and J. L. Prince, "Improving magnetic resonance resolution with supervised learning," in *Proc. IEEE 11th Int. Symp. Biomed. Imag. (ISBI)*, Apr./May 2014, pp. 987–990.

**KE XU** is currently pursuing the M.S. degree with the School of Digital Media, Jiangnan University, Wuxi, China. His research interests include pattern recognition as well as bioinformatics.

**JIAWEI CAO** is currently pursuing the M.S. degree with the School of Digital Media, Jiangnan University, Wuxi, China. His research interests include pattern recognition and data mining.

**KAIJIAN XIA** received the M.S. degree in computer science and technology from Jiangnan University, in 2009. He is currently pursuing the Ph.D. degree with the China University of Mining and Technology. From 2009 to 2010, he was a Lecturer with the School of Computer Science and Engineering, Changshu Institute of Technology. Since 2010, he has been with Changshu No.1 People's Hospital. He has published over 20 articles in international/national journals. His research interests include biological image processing and computational medicine.

**HUAN YANG** is currently pursuing the M.S. degree with the School of Digital Media, Jiangnan University, Wuxi, China. Her research interest includes deep learning and its applications.

**JUNQING ZHU** received the bachelor's degree in physics from the Shanghai University of Science and Technology, Shanghai, China, in 1989. In 2006, he joined Case Western Reserve University, where he is currently a Senior Staff of radiology. In the past three decades, he has been focused on in vivo molecular imaging. He currently involved in special emphasis on molecular imaging in neurodegenerative diseases, such as multiple sclerosis (MS), Alzheimer's disease (AD), Parkinson's disease, Epilepsy disease, and DNA damage and repair in cancer. By continuously working with Molecular Imaging Probe Group, he pioneered imaging of myelin based on different imaging modalities, such as PET, MRI, and near-infrared fluorescence imaging.

**CHUNYING WU** received the Ph.D. degree in imaging medicine and nuclear medicine from the School of Medicine, Fudan University, Shanghai, China, in 2003. In 2004, she was a Postdoctoral Fellow with the University of Illinois at Chicago. In 2006, she joined Case Western Reserve University, where she is currently an Instructor of radiology with the Division of Molecular Imaging Center, Case Center for Imaging Research, School of Medicine. She has extensive experience in radiopharmaceutical development for PET and SPECT imaging. Over the past ten years, her research has focused on the development of small-molecular probes for PET imaging in Alzheimer's disease, multiple sclerosis, and DNA damage and repair in cancer. Her research was selected for Molecular Imaging/CMIIT Basic Science and Neuroscience Summary Session highlight talk in the society of nuclear medicine (SNM) annual meeting, in 2013 and 2016. Some of her work has also been selected twice as the second place in the poster competition at the annual SNM conferences.

**YIZHANG JIANG** received the Ph.D. degree from Jiangnan University, in June 2016. He is currently an Instructor with the School of Digital Media, Jiangnan University, Wuxi, China. He has been a Research Assistant with the Computing Department, The Hong Kong Polytechnic University, for more than one year. He has published more than 20 articles in international journals, including the IEEE TFS, the IEEE TNNLS, the IEEE TRANSACTIONS ON CYBERNETICS, and *Information Sciences*. His research interests include pattern recognition, intelligent computation, and their applications.

**PENGJIANG QIAN** received the Ph.D. degree from Jiangnan University, in March 2011. He is currently a Full Professor with the School of Digital Media, Jiangnan University, Wuxi, China. He has authored or coauthored more than 70 articles published in international/national journals and conferences, such as the IEEE TNNLS, the IEEE TSMC-B, the IEEE TFS, the IEEE TRANSACTIONS ON CYBERNETICS, and *Pattern Recognition*. His research interests include data mining, pattern recognition, bioinformatics, and their applications, such as analysis and processing for medical imaging, intelligent traffic dispatching, and advanced business intelligence in logistics.